Journal of Power Sources 219 (2012) 317–324

Contents lists available at SciVerse ScienceDirect

Journal of Power Sources

journal homepage: www.elsevier.com/locate/jpowsour

Thermal regenerative design of a fuel cell cogeneration system

Jenn-Jiang Hwang*

Department of Greenergy, National University of Tainan, Tainan, Taiwan

HIGHLIGHTS

- The thermal regenerative unit recovers the heat dissipated by the stack.
- A thermostat valve has optimized the stack operation temperature.
- The effectiveness of the planar heat exchanger rounds 100% in the steady state.
- The thermal efficiency of the fuel cell cogeneration system is about 20 ± 8%.
- The overall efficiency of the cogeneration system is as high as 75% at $P_L = 2.5$ kW and $T_R = 54$ °C.

ARTICLE INFO

Article history:
Received 11 June 2012
Received in revised form
21 July 2012
Accepted 23 July 2012
Available online 1 August 2012

Keywords:
Proton exchange membrane fuel cell
Thermostat
Efficiency
Cogeneration system

ABSTRACT

The objective of the present work is to design and fabricate a thermal management system (TMS) that commands a proton exchange membrane fuel cell (PEMFC) based cogeneration system to generate the electricity and hot water efficiently. Parametric studies include the external load (P_L) and the regenerative temperature (T_R). A thermostat valve is employed to optimize the stack operation temperature, while a thermal regenerative unit (TRU) containing a planar heat exchanger is used to recover the heat dissipated by the stack. First, the dynamics of thermal and electrical characteristics such as voltage, current, power, coolant temperature, coolant flow rate, and hydrogen flow rate are measured to check the reliability of the TMS. Then, the effectiveness of the planar heat exchanger is determined to verify the cooling ability of the TRU. Moreover, the transient system efficiencies, including electrical efficiency, thermal efficiency, and overall efficiency are determined. Furthermore, the effect of the regenerative temperature on the time-averaged system efficiencies is examined under different external loads. Finally, an empirical correlation for time-averaged overall efficiency is proposed for helping in design of the PEMFC cogeneration system.

1. Introduction

A variety of technologies are available to provide heating and electricity to our homes [1]. Combined heat and power (CHP), also known as cogeneration, is the term used for when electricity and heat are co-produced from a single fuel source such as natural gas, coal, or oil. When the CHP is done on a residential scale, it can replace or supplement grid electricity as a form of distributed generator in users' residences, and producing energy onsite avoids transmission losses.

Fuel cells are quite suitable to residential CHP, because the technology inherently produces both electricity and heat from household fuels such as liquid petroleum gas (LPG) and natural gas [2–4]. The electrical efficiency of a fuel cell is higher than conventional electricity generation, typically over 45% compared to 25–35% for fossil-fuel combustion in a conventional power plant. When the heat is used, the overall efficiency of fuel conversion can approach 90%. This means that greenhouse gas emissions could be significantly reduced. In addition, these fuel cell systems can complement other domestic renewable energy generation such as solar PV panels [5]. They are also eligible for feed-in tariffs, allowing any excess electricity to be sold to the grid, although it is not general conditions and is bounded to high variability along different local regulations.

Due to the significant technology advances made recently [6] and good match for the thermal/electric (T/E) load ratios [7], proton exchange membrane fuel cells (PEMFCs) based cogeneration systems are considered to be in the forefront of all types of fuel cells for residential application. In this application PEMFCs run during the day when electricity demand is higher and can be switched off at night when electricity and hot water demand is low. This cycling can be done without harming the fuel cell and increases the overall

* Tel./fax: +886 62602251.
E-mail address: azaijj@mail.nutn.edu.tw.

0378-7753/$ – see front matter © 2012 Elsevier B.V. All rights reserved.
http://dx.doi.org/10.1016/j.jpowsour.2012.07.069

efficiency of the system. Besides, solid oxide fuel cell (SOFCs) are also being introduced to residential CHP schemes, with efficiencies on a par with PEMFC cogeneration systems, but they should be run as continuously as possible in order to prolong the lifetime of the system. Because SOFCs run at higher operating temperatures than PEMFCs, they are more tolerant of carbon monoxide in fuels, which allows for some simplification of the system configuration. Nowadays, both types are available in the ENE-FARM scheme [8,9], the Japanese government supported commercialization program of fuel cells in residential CHP.

Although, a large amount of research works, experimental or theoretical, have been conducted to study the performance of fuel cell cogeneration systems in the past decade [10–23], measurements of transient thermal-electrical characteristics in a PEMFC cogeneration system are still sparse in the open literature. Therefore, we set the objective of the present work to design and fabricate an experimental setup for a PEMFC cogeneration capable of monitoring the operating conditions during non-steady state operation. First, a thermal management system (TMS) that thermally manages a PEMFC-based cogeneration system is developed, which not only recovers the heat dissipated by the stack but also maintains the stack optimum operating temperature. The TMS comprises a stack coolant circuit and a thermal regenerative unit (TRU). A planar heat exchanger interfaces between the stack coolant circuit and the TRU that facilitates the heat recovery from the hot stack coolant to the cold tap water. A thermostat is employed to control the stack coolant flow to TRU so that the stack could maintain its optimum operating temperature. After implementing the TMS on the fuel cell generator, the thermal and electrical characteristics of the fuel cell cogeneration system are measured and discussed in detail. Then, the effectiveness of the planar heat exchanger is determined by using the stack coolant temperature and the tap water temperature. Moreover, the effects of external loads and regenerative temperatures on the system efficiencies, including electrical efficiency, thermal efficiency, and overall efficiency, are examined. Finally, an empirical correlation for averaged overall efficiency is proposed for future design of the PEMFC cogeneration system.

2. Experimental apparatus

2.1. Principle of cogeneration

The overall reaction in a PEMFC is a combination of the hydrogen oxidation reaction (HOR) in anode and the oxygen reduction reaction (ORR) in cathode. They can be expressed by the following equations:

$$\text{Anode reaction}: H_2 \rightarrow 2H^+ + 2e^- \quad (1)$$

$$\text{Cathode reaction}: 2H^+ + 1/2O_2 + 2e^- \rightarrow H_2O \quad (2)$$

$$\text{Overall reaction}: H_2 + 1/2O_2 \rightarrow H_2O + \text{Heat} \quad (3)$$

Therefore, a PEMFC produces electricity based on the electrochemical reaction. Essentially, its operation does not involve fuel combustion with huge thermal energy release. However, the overall reaction in Eq. (3) is exothermic with heat as byproducts. Therefore, when the released heat could be coupled for space and domestic hot water heating for residential, commercial or institutional applications, the PEMFC system is an exact cogeneration system.

2.2. Electrical power generator

Fig. 1 gives a schematic drawing of a fuel cell cogeneration system. Basically, it comprises a PEMFC-based electrical power generator and a thermal management system (TMS) recovering the thermal energy dissipated by the fuel cell stack and controlling the stack at its optimum operating temperature. Photographs shown in Fig. 2 are the experimental setup of the fuel cell cogeneration system. The heart of the fuel cell cogeneration system is a home-mode PEMFC stack. Its technical specifications are listed in Table 1.

As shown in Fig. 1, the air supply subsystem provides filtered, conditioned air to the fuel cell stack. The cathode air blower using load-following schemes controls the airflow rate to the stack cathode at a fixed stoichiometry of 2.5. A hollow-fiber membrane humidifier recovers heat and humidity from the cathode exhaust gases to the fresh airstream from the cathode inlet. In the hydrogen delivery subsystem, pure hydrogen feeds the stack anode for electrochemical oxidation reaction. Then, the unreacted hydrogen is pumped back to the hydrogen pipeline at the stack anode inlet [24,25]. The bypass of the anode exhaust is equipped with a solenoid valve to conditionally purge exhausts and inert to the inlet of the stack cathode. Since the hydrogen pipeline in the stack anode is a closed loop, the hydrogen delivery depends on the hydrogen pressure in the anode [26]. During operation of the fuel cell system, the hydrogen pressure in the stack anode decreases gradually due to HOR. When the anode hydrogen pressure is lower than a pre-set value, the solenoid valves on the hydrogen pipeline ahead of the

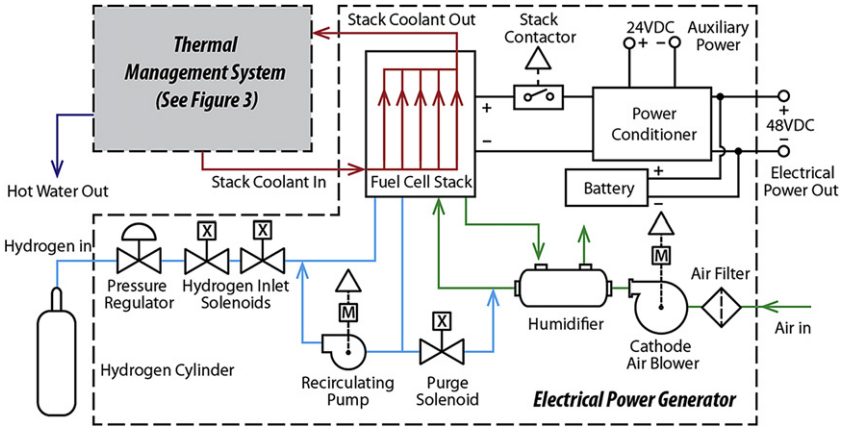

Fig. 1. Schematic drawing of the fuel cell cogeneration system.

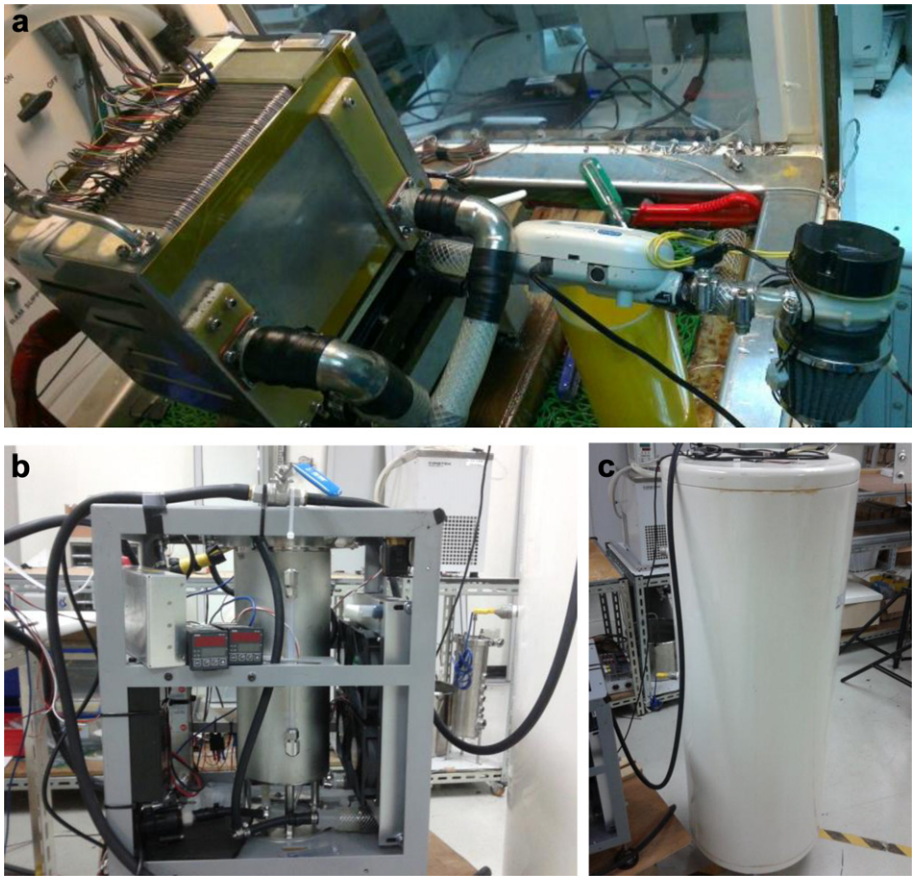

Fig. 2. Photos of the experimental setup of fuel cell cogeneration system, (a) fuel cell stack, (b) thermal regenerative unit, (c) hot water reservoir.

stack opens to feed the anode with hydrogen that increases the hydrogen pressure. Then, the solenoid valves shut and the hydrogen pressure in the anode decreases due to HOR again. Consequently, the control strategy of anode hydrogen delivery is to switch the solenoid valves on/off again and again that keeps the anode hydrogen pressure in a pre-set range; thus feeding the stack anode with hydrogen.

As shown in Fig. 1, a power conditioner interfaces between the fuel cell stack power and the external load. Major components include a solid-state boost/buck converter module, an electronic load together with distribution hardware, and a power controller. To provide quick-response power to variable loads, the fuel cell stack couples with a lithium-ion battery in the present work [26,27]. When the fuel cell stack is operating, the stack power is boosted to positive 48VDC by the converter module for external load, and part power is bucked to positive 24VDC for the auxiliary power. When the power deficiency/excess occurs due to load variations, the converter module could regulate the power flow from/to the lithium-ion battery. For example, during the high power demand conditions, the converter module boosts the stack power to the external load and meanwhile the battery discharges to add extra power to the load as well. In contrast, when the stack power is larger than the power demand by the external load, the converter module boosts the stack power to provide the power to the external load, and the extra stack power is used to charge the lithium-ion battery. Note that because of the slow dynamics of fuel cell stack, it does not deliver its power during the startup instant; instead, the lithium-ion battery discharges its current to power the auxiliary components through the converter module.

Table 1
Brief technical specifications of the fuel cell stack.

Specifications	Value
Number of cells	63
Active area	225 cm^2
Rated power	4000 W
Maximum power	5800 W
Operating voltage range	42–60 VDC
Operating current range	0–120 A
Anode feeding	Gaseous hydrogen, 99.95% in purity
Cathode feeding	Ambient air
Pt-loading, cathode	0.2 mg cm^{-2}
Pt-loading, anode	0.15 mg cm^{-2}
Bipolar plate material	Plastic–graphite composite
Flow field type	Serpentine
Membrane	Nafion® 117

2.3. Thermal management system

There are two goals in design of the thermal management system of a fuel cell generator. The first one is to control the stack operation temperature in its optimum range. The second goal is to recover the wasted thermal energy dissipated by the stack efficiently.

Fig. 3 illustrates schematically the thermal management system, which comprises a stack coolant circuit and a thermal regenerative unit. Major components used in the thermal management system are list in Table 2.

The stack coolant used herein is a mixture of 50% propylene glycol and 50% DI water. As shown Fig. 3, a coolant pump pumps the

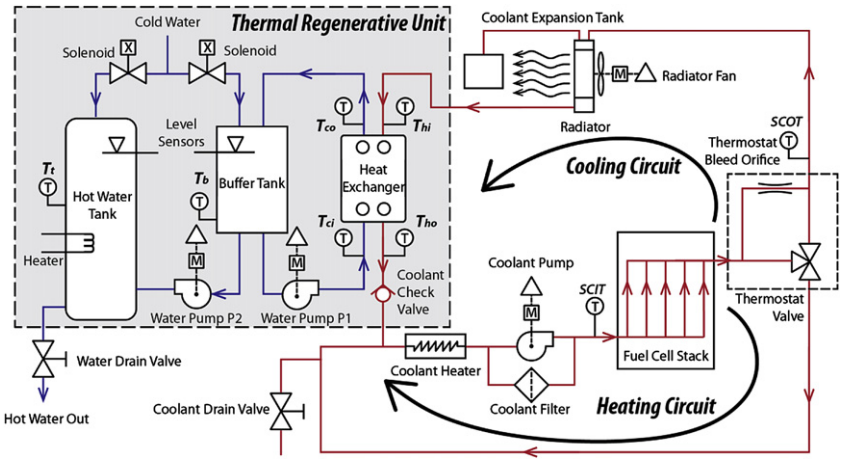

Fig. 3. Schematic drawing of the thermal management system (TMS).

coolant through the parallel channels in the stack to remove the heat dissipated by the stack. The stack coolant then enters a thermostat, which is a three-way valve that distributes the coolant flow into two streams, i.e., the cooling circuit and the heating circuit. A temperature sensor on the stack coolant circuit ahead of the stack monitors the stack coolant inlet temperature (SCIT), which is used as the control point for the thermostat, the coolant heater, and the water pump P1. Technically, to ensure that a stack is always operating at its optimum temperature, the thermostat modulates it's opening to distribute the coolant streams in two coolant circuits. The coolant in the cooling circuit is cooled by the planar heat exchanger and returned to mix with that circulating through the heater to maintain a pre-set SCIT before entering the stack. In the present control strategy, the thermostat begins to open the cooling stream when the SCIT reaches 50 °C. At SCIT = 60 °C it is fully open, allowing the stack coolant to pass through the cooling circuit totally. When the system starts, to ensure that the stack reaches its optimum-operating temperature as quickly as possible, the thermostat restricts the coolant flow from the stack to the cooling circuit to virtually zero. Therefore, all stack coolant is heated in the heating circuit until the stack reaches its optimum operating temperature. Note that a small flow of stack coolant through the bleed orifice from the stack to the cooling circuit is required so that the thermostat experiences changes to the coolant temperature as the stack warms up. Subsequently, the coolant heater is turned off and the thermostat gradually opens up to allow sufficient coolant to flow through the cooling circuit to remove the heat being produced by the stack and prevent the stack temperature rising higher. In addition, the water pump P1 modulates its speed to stabilize the stack operation temperature. At a fixed stack coolant flow rate in the cooling circuit, if the SCIT increases higher than the pre-set value, the water pump P1 speeds up to remove more heat from the stack coolant. On the contrary, the water pump P1 will slow down when the SCIT decreases lower than the pre-set value.

Table 2
Components used in the thermal management system.

Components	Quantity
Fuel cell stack	1
Temperature sensor	8
Flow sensor	3
Liquid level sensor	3
Thermostat valve	1
Solenoid valve	3
Radiator with turbofan	1
Coolant pump	1
Coolant heater	1
Coolant filter	1
Coolant expansion tank	1
Water pump	2
Check valve	3
Gas vent valve	1
Open loop current sensor	4
Ball valve	1
Buffer tank	1
Planar heat exchanger	1
Hot water tank with heater	1
Microcontroller	1

The water temperature in the buffer tank T_b increases gradually during operation. When the water temperature in the buffer tank increases higher than a pre-set value (known as regenerative temperature T_R), the water pump P2 begins to pump the hot water in the buffer tank to the hot-water reservoir. Meanwhile, the cold tap water is fed into the buffer tank to keep the water level. It stops pumping the hot water as long as the water temperature reduces lower than the regenerative temperature, $T_b < T_R$. Consequently, the water reservoir collects hot water from the buffer tank from time to time. If the water temperature in the hot water reservoir decreases to the regenerative temperature, the electrical heater is switched on to keeps the water in the reservoir from cooling. Thus, the fuel cell cogeneration system can always supply hot water of regenerative temperature to users. In the present work, three different regenerative temperatures, i.e., T_R = 48 °C, 50 °C, and 54 °C, are investigated to examine their effect on the thermal efficiency of the fuel cell cogeneration. It is also noted that when the hot-water tank is full and no hot water is consumed, the author's previous work [21,22] dumps extra heat by draining out hot water to keep fuel cell cooling. In the present design, an additional radiator together with a turbofan is installed in the cooling circuit (Fig. 3). As long as hot-water tank is full, the water pump P1 is turned off, and simultaneously the radiator turbofan starts working to keep fuel cell cooling.

3. Results and discussion

3.1. Electrical characteristics

Fig. 4 shows the electrical dynamics of the fuel cell cogeneration system under a step change in system power. The system is turned on at $t = 0$, keeps standby before $t = 900$ s, then delivers power of 2.35 kW for 1 h, and finally shuts down at $t = 4500$ s. It is seen that the stack power is varied largely when the system is extracted

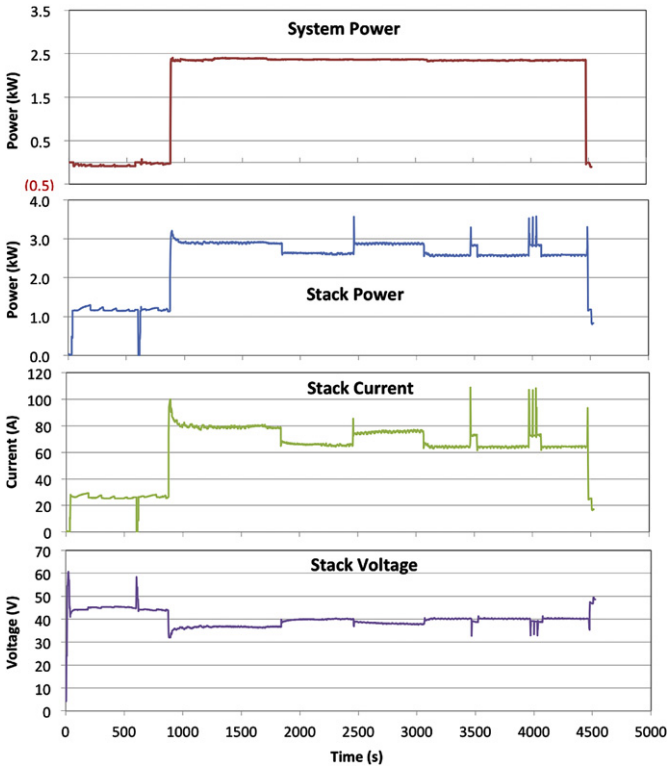

Fig. 4. Electrical dynamics of the fuel cell cogeneration system, T_R=50°C.

a constant system power. In addition, the stack power is always higher than the system power. The extra power is mainly used to drive the system auxiliaries. It is further seen that the dynamics of the current extracted form the stack is similar to those of the stack power. While, the stack voltage is ranged from its OCV (60VDC) to its cut-off voltage, depending on the current extracted from the stack.

Fig. 5 shows the dynamics of the hydrogen usage corresponding to the system power in Fig. 4. In general, the dynamics of hydrogen usage is parallel with the current dynamics shown in Fig. 4. From Eq. (1), basically, the hydrogen usage is proportional to the protons (also current) through the fuel cell stack during the reaction. Therefore, the current passing through the fuel cell can represent the hydrogen consumption rate. Noteworthy that the system consumes hydrogen of about 20 LPM but without any output in electrical power in standby, which reflects null in the electrical efficiency and will be shown later.

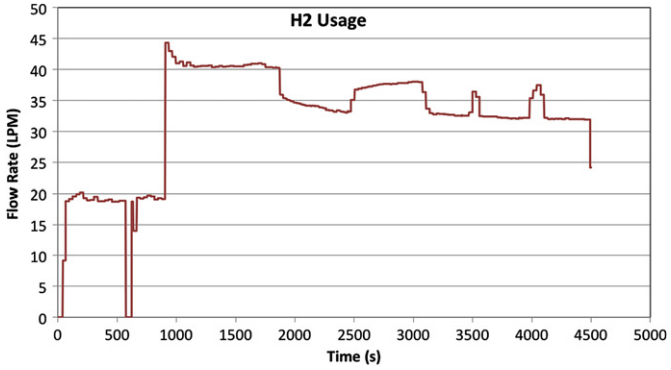

Fig. 5. Dynamics of the hydrogen consumption rate, T_R=50°C.

3.2. Thermal characteristics

In general, a PEM fuel cell runs optimally with a temperature about 80 °C. However, it is hard to identify the real temperature inside the stack during operation because the in-situ measuring technology is not available yet. Alternatively, the present work controls the fuel cell operation temperature through regulating the stack coolant inlet temperatures (SCITs). According to the simulation results [28–30], the fuel cell operation temperature would be about 10–20 °C higher than the SCIT. The SCIT is therefore controlled at 60 °C in the present work. Technically, the microcontroller controls the SCIT through coordinating the activities of the coolant heater, the water pump, and degree of opening of the thermostat.

Fig. 6 shows the relationship between the distribution of SCIT and the heating/cooling activities of the TMS, which has clearly illustrated the thermal control scheme employed in the present work. It is seen from this figure that because the stack is producing little heat when the system keeps in standby ($t < 900$ s), the coolant heater is acting to warm up the coolant to ensure that the stack reaches optimum-operating temperature as quickly as possible. When the SCIT is higher than the pre-set temperature 55 °C ($t > 900$ s), the coolant heater is turned off and the water pump P1 is acting promptly to remove the heat from the hot stack coolant. Hereafter, the water pump P1 modulates its speed to control the stack coolant temperature. It remains on during the period of 1600 s–2200 s because of the transition to the steady state from the unstable conditions. In addition, the little ripples distributed on the SCIT profile are consistent with the actuations of the water pump P1. Actually, the water-pump speed is a vital factor of the system efficiency. When the water-pump speeds are too slow, poor cooling will cause malfunction of the fuel cell stack. Conversely, when the water pump runs too fast, the cold coolant reduces the stack temperature that will depart from its optimum operation conditions. In addition, it will consume more pumping power. Both factors do not favor the electrical efficiency.

As further seen in Fig. 6, the present work has successfully employed the pulse width modulation (PWM) schemes to regulate

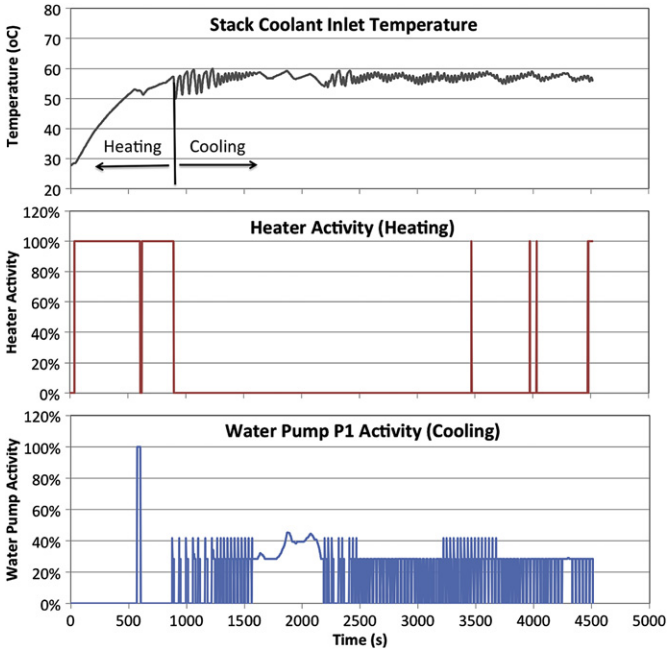

Fig. 6. Thermal control of the fuel cell cogeneration system, T_R=50°C.

the pump speed to confine the SCIT around 57 ± 2 °C in the steady state (2500 s < t < 4500 s). Basically, the PWM is an innovative control scheme that can be used with a various pump types including multi-stage, single-stage, surface and submersible pumps. It is energy saving, silent running, and can extend the life of the pump [31]. According to the specification provided by the manufacturer, the durability of a pump with such a power cycling could reach as high as 25,000 h.

Fig. 7 further shows the dynamics of the flow rates of the stack coolant and the cooling water in the steady state (2500 s < t < 4500 s). As shown in Fig. 7, most of the stack coolant is circulated into cooling circuit (i.e., heat exchanger), typically about 1.9–4.3 LPM. As for the cooling water, it has pulse values of 2.7 LPM intermittently. From the above flow dynamics, it can be clearly seen that the control schemes using in coolant flow rates and water flow rates are different. In the present design, the stack coolant is pumped across the stack with a constant speed (flow rate), and the proportion of coolant circulated around the heating circuit versus the proportion sent to the cooling circuit is determined by the degree of opening of the thermostat. As for the water flow rate, it is adjusted by using the PWM scheme to control the water pump speed. In general, the coolant flow rate compromises the water flow rate based on the optimum stack coolant inlet temperature.

Fig. 8 shows the dynamics of fluid temperatures across the planar heat exchanger when the stack cooling is active (t > 900 s). The fluid temperatures on the four ports of the heat exchanger are denoted on Fig. 3. It is seen from this figure that the hot coolant inlet temperature T_{hi} (red curve) is relatively stable, ranging from 78 ± 1 °C in the steady state (2500 s < t < 4500 s). It significantly reduces to 48 ± 2 °C as hot coolant passes through the planar heat exchanger. In addition, the water outlet temperature T_{co} (green curve) is stable as well while the water inlet temperature T_{ci} (blue curve) is largely fluctuated because of the pour of cold tap water into the buffer tank.

From the above measurements of fluid temperatures and flow rates, the heat exchanger effectiveness can be determined, which is defined as the heat transfer rate in the real case (q) to that in a perfect heat exchanger (q_{max}), and can be expressed by the following equation.

$$\eta_{HX} = \frac{q}{q_{max}} = \frac{m_h C_{p,h}(T_{hi} - T_{ho})}{(mC_p)_{min}(T_{hi} - T_{ci})} = \frac{T_{hi} - T_{ho}}{T_{hi} - T_{ci}} \quad (4)$$

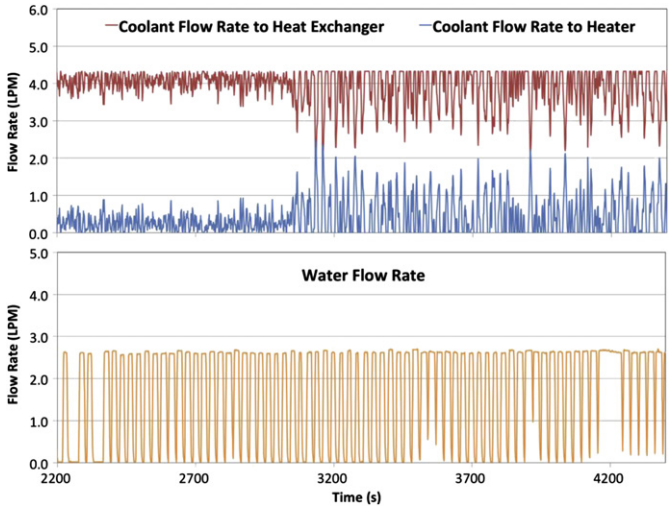

Fig. 7. Comparison of coolant flow rates and water flow rate, T_R=50°C.

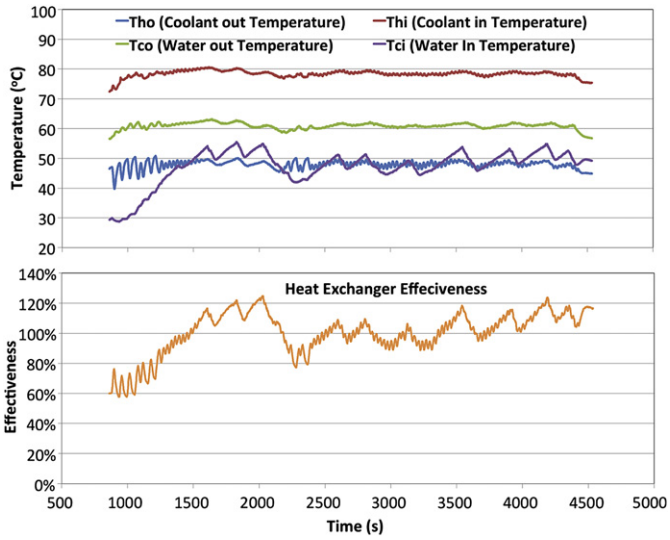

Fig. 8. Dynamics of the coolant and water temperature, and heat exchanger effectiveness, T_R=50°C.

where m_h (kg-s^{-1}) is the coolant flow rate, $C_{p,h}$ (kJ-kg^{-1}-K^{-1}) is the specific heat capacity of the coolant, and $(mC_p)_{min}$ in the denominator of Eq. (4) is also the coolant circuit. From Fig. 8 it is observed that the heat exchanger effectiveness rounds 100%, even instantly above this. This is due to the transient operation of the heat exchanger that leads to cyclic accumulation of thermal energy in the metallic plates and body of the heat exchanger.

3.3. System efficiency

In the present work, three kinds of system efficiencies are measured and discussed, i.e., thermal efficiency, electrical efficiency, and overall efficiency. The thermal efficiency is defined as the ratio of the thermal power recovered by cold water from the heat dissipated by the electrochemical reaction in the fuel cell stack to the hydrogen power consumption. Accordingly, it can be reported as:

$$\varepsilon_T = \frac{P_T}{P_{H2}} = \frac{v_w \times (\rho_w \times C_{p,w} - \Delta T)}{n_{H2} \times \Delta h} \quad (5)$$

where v_w (m^3 s^{-1}) is the water flow rate, ρ_w (kg m^{-3}), the water density, $C_{p,w}$ (kJ-kg^{-1}-K^{-1}), the specific heat capacity of water, ΔT (K), the water temperature difference between the heat exchanger outlet and inlet, n_{H2} (mol-s^{-1}), the hydrogen consumption rate, and, Δh (kJ mol^{-1}), the hydrogen enthalpy based on the lower heating value (LHV). As for the electrical efficiency of the fuel cell cogeneration system, it can be expressed as:

$$\varepsilon_E = \frac{P_E}{P_{H2}} = \frac{I \times V}{n_{H2} \times \Delta h} \quad (6)$$

where P_E is the net electrical power output to the external load from the fuel cell cogeneration system, which is a direct measure of voltage (V) across the external load and the current (I) passing through the external load. The overall efficiency illustrates how much total useful power gains from the consumed hydrogen power, which is expressed as:

$$\varepsilon_{CHP} = \varepsilon_T + \varepsilon_E \quad (7)$$

Fig. 9 shows the dynamics of electrical efficiency, thermal efficiency, and overall efficiency of the fuel cell cogeneration system in

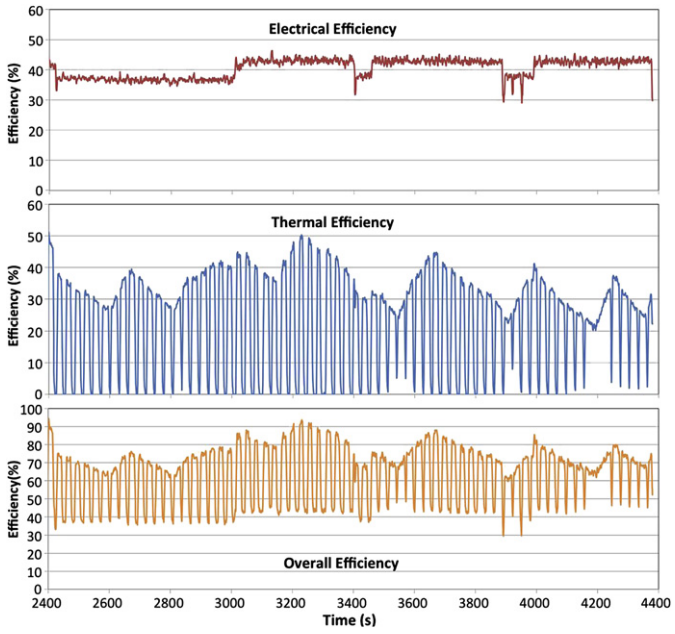

Fig. 9. Dynamics of electrical efficiency, thermal efficiency, and cogeneration efficiency in the steady state.

the steady state (2500 s $< t <$ 4500 s). It is seen from Fig. 9(a) that the electrical efficiency steps between 38% and 42% due to the change in the auxiliary power. As for the thermal efficiency, the distributions are largely fluctuated, which are subjected to the pulse dynamics of the water flow rate shown in Fig. 7, which is attributed to the operational mode of the water pump. Typically, the valleys on the distribution are virtually zero because of null in the water flow rate. The peaks of the pulse distribution of the thermal efficiency ranges between 24% and 50%, which means that about quarter to half hydrogen chemical energy is transferred into useful thermal energy by the present thermal management system. Consequently, in combination of the output electrical energy and the thermal recovery energy, the dynamic overall efficiency of the present fuel cell cogeneration system ranges from 30% to 95% under the constant external load of 2.35 kW.

Fig. 10 shows the time-averaged system efficiencies as a function of the external load under various regenerative temperatures, i.e., $T_R = 48\,^{\circ}C$, 50 °C and 54 °C, respectively. They are averaged over the time interval of 2500 s $< t <$ 4500 s. From this figure it is seen that the electrical efficiency increases with increasing the external load, while the thermal efficiency is relatively unaffected by the external load. The overall efficiency of the present fuel cell cogeneration system reaches 75% during the range of the external load investigated. Fig. 11 re-collects the data reported in Fig. 10 to illustrate the effect of regenerative temperature T_R. It is clearly seen from Fig. 11 that the effect of T_R on the average electrical efficiency is quite small and thus negligible. It is very reasonable since the electrical efficiency of the fuel cell generator should be consistent regardless of the cooling technology employed. Actually, the consistency in the electrical efficiency under various T_R has verified the reliability of the thermal management system developed in the present work. In contrast, the data of thermal efficiency are somewhat scattered. Anyway, they are ranged from 28 ± 8% during the range of the external load investigated. As for the overall efficiency, the data can be curve-fit as the following equation:

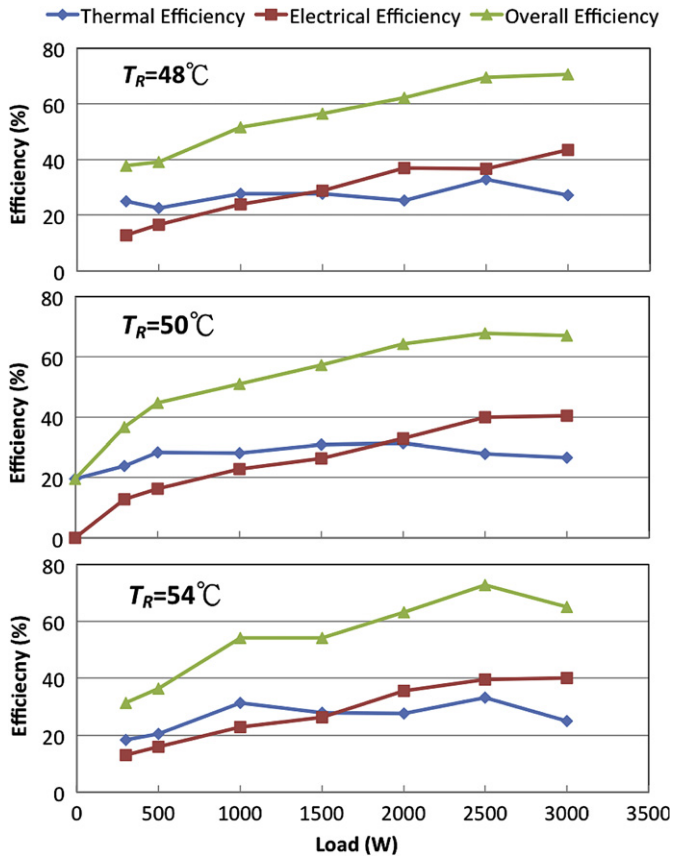

Fig. 10. Load effects on the time-averaged efficiencies of the fuel cell cogeneration system for different regenerative temperatures.

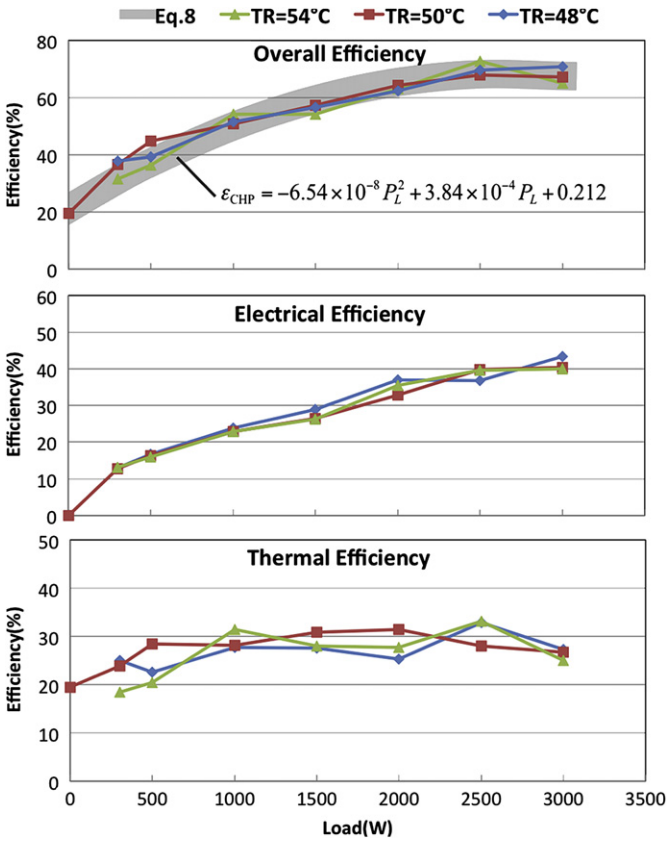

Fig. 11. Correlation for the time-averaged overall efficiency of the fuel cell cogeneration system.

$$\varepsilon_{CHP} = -6.54 \times 10^{-8} P_L^2 + 3.84 \times 10^{-4} P_L + 0.212 \quad (8)$$

where P_L (W) is the external load exerted on the fuel cell cogeneration system. The maximum deviation of the above equation and the experimental data is less than 5%, which is shown by the data band in Fig. 11.

4. Conclusion

The present work has successfully designed and fabricated a thermal management system that controls well a PEMFC cogeneration system thermally. Transient data of electrical and thermal-fluid characteristics such as voltage, current, power, coolant temperature, coolant flow rate, and hydrogen flow rate are presented, which have proved the reliability of the present scheme. Major findings derived from the above measurements are summarized below.

1. The thermal management system along with smart thermal control algorisms has managed the fuel cell cogeneration system properly. It does not only well control the stack coolant inlet temperature (SCIT) but also recover the thermal energy efficiently.
2. The thermostat keeps the stack from overheating by allowing hot stack coolant to flow into the cooling circuit thus reducing stack-operating temperature. Conversely, when the stack is operated below its optimum temperature, the thermostat directs the stack coolant flowing into the heating circuit to facilitate the stack warm-up.
3. The dynamics of thermal efficiency are largely dependent on the actuation of the water pump P1, while the transient electrical efficiency distribution is mainly shaped by the auxiliary power of the cathode air blower and the coolant heater.
4. The time-averaged electrical efficiency is relatively unaffected by the regenerative temperature. In contrast, the time-averaged thermal efficiency is scattered from 20% to 36% for different regenerative temperatures.
5. During the external-load range of $0 < P_L < 3.0$ kW, the time-averaged electrical efficiency is increased with increasing the external load, while the time-averaged thermal efficiency is ranged from $28 \pm 8\%$. Consequently, the time-averaged overall efficiency is increased with increasing external load and can reach as high as 75% at $P_L = 2.5$ kW and $T_R = 54\ ^\circ$C.

Acknowledges

The author professor Jenn Jiang Hwang would like to thank the National Science Council of Taiwan, for financially supporting this research under contract no. NSC 94-2212-E-451-001.

References

[1] N. Petchers, Combined Heating, Cooling & Power Handbook: Technologies & Applications: An Integrated Approach to Energy Resource Optimization, Fairmont Press, October 16, 2002.
[2] W.M. Ellis, M.B. Gunes, ASHRAE Trans. (2002) 108–111.
[3] K. Krist, J.D. Wright, Solid Oxide Fuel Cell Residential Cogeneration, 1999 Joint DOE/EPRI/GRI FC Technology Review Conference, Chicago, USA, 1999.
[4] Q. Okada, K. Yokoyama, Fuel Cells 1 (2001) 72–77.
[5] J.J. Hwang, L.K. Lai, W. Wu, W.R. Chang, Int. J. Hydrogen Energy 34 (2009) 9531–9542.
[6] P. Costamagna, S. Srinivasan, J. Power Sources 102 (2001) 242–252.
[7] W. Collella, J. Power Sources 106 (2002) 388–396.
[8] D. Carter, Fuel Cell Today 29 (Feb. 2012).
[9] Japanese group unveils SOFC Ene-Farm residential cogen unit, Fuel Cells Bull. 4 (2012).
[10] E. Entchev, J. Power Sources 118 (2003) 212–217.
[11] A. Ferguson, V.I. Ugursal, J. Power Sources 137 (2004) 30–42.
[12] G. Gigliucci, L. Petruzzi, E. Cerelli, A. Garzisi, A. La Mendola, J. Power Sources 131 (2004) 62–68.
[13] P. König, A. Weber, N. Lewald, T. Aicher, L. Jörissen, E. Ivers-Tiffée, et al., J. Power Sources 145 (2005) 327–335.
[14] M.D. Paepe, P. D'Herdt, D. Mertens, Energy Convers. Manage. 47 (2006) 3435–3446.
[15] M. Radulescu, O. Lottin, M. Feidt, C. Lombard, D. Le Noc, S. Le Doze, J. Power Sources 159 (2006) 1142–1146.
[16] S. Obara, Int. J. Hydrogen Energy 31 (2006) 1807–1818.
[17] H.S. Chu, F. Tsau, Y.Y. Yan, K.L. Hsueh, F.L. Chen, J. Power Sources 176 (2008) 499–514.
[18] S. Campanari, E. Macchi, G. Manzolin, Int. J. Hydrogen Energy 33 (2008) 1361–1373.
[19] A.D. Hawkes, D.J.L. Brett, N.P. Brandon, Int. J. Hydrogen Energy 34 (2009) 9545–9557.
[20] K. Maeda, K. Masumoto, A. Hayano, J. Power Sources 195 (2010) 3779–3784.
[21] J.J. Hwang, M.L. Zou, J. Power Sources 195 (2010) 2579–2585.
[22] J.J. Hwang, M.L. Zou, Int. J. Hydrogen Energy 35 (2010) 8644–8653.
[23] N. Briguglio, M. Ferraro, G. Brunaccini, V. Antonucci, Int. J. Hydrogen Energy 36 (2011) 8023–8029.
[24] J.J. Hwang, D.Y. Wang, N.J. Shih, J. Power Source 141 (2005) 108–115.
[25] J.J. Hwang, W.R. Chang, A. Su, F.B. Weng, Int. J. Hydrogen Energy 33 (2008) 3801–3807.
[26] J.J. Hwang, W.R. Chang, J. Power Sources 207 (2012) 111–119.
[27] J.J. Hwang, W.R. Chang, J. Chinese Soc. Mech. Eng. 32 (2011) 181–187.
[28] J.J. Hwang, J. Electrochem. Soc. 153 (2006) A216–A224.
[29] J.J. Hwang, P.Y. Chen, Int. J. Heat Mass Transfer 49 (2006) 2315–2327.
[30] J.J. Hwang, C.H. Chao, Int. J. Hydrogen Energy 32 (2007) 405–414.
[31] Hydraulic Institute and Europump, Variable Speed Pumping – a Guide to Successful Applications, Elsevier Advanced Technology, UK, 2005.